Physics of knuckleballs

New Journal of Physics
The open access journal at the forefront of physics

Deutsche Physikalische Gesellschaft DPG
IOP Institute of Physics

Published in partnership with: Deutsche Physikalische Gesellschaft and the Institute of Physics

OPEN ACCESS

RECEIVED
18 December 2015

REVISED
6 June 2016

ACCEPTED FOR PUBLICATION
20 June 2016

PUBLISHED
13 July 2016

PAPER

Physics of knuckleballs

Baptiste Darbois Texier[1], **Caroline Cohen**[1], **David Quéré**[2] **and Christophe Clanet**[1,3]

[1] LadHyX, UMR 7646 du CNRS, Ecole Polytechnique, 91128 Palaiseau Cedex, France
[2] PMMH, UMR 7636 du CNRS, ESPCI, 75005 Paris, France
[3] Author to whom any correspondence should be addressed.

E-mail: clanet@ladhyx.polytechnique.fr

Keywords: sport ballistics, zigzag trajectory, path instability, drag crisis, symmetry breaking

Abstract

Zigzag paths in sports ball trajectories are exceptional events. They have been reported in baseball (from where the word knuckleball comes from), in volleyball and in soccer. Such trajectories are associated with intermittent breaking of the lateral symmetry in the surrounding flow. The different scenarios proposed in the literature (such as the effect of seams in baseball) are first discussed and compared to existing data. We then perform experiments on zigzag trajectories and propose a new explanation based on unsteady lift forces. In a second step, we exploit wind tunnel measurements of these unsteady lift forces to solve the equations of motion for various sports and deduce the characteristics of the zigzags, pointing out the role of the drag crisis. Finally, the conditions for the observation of such trajectories in sports are discussed.

1. Introduction

In many sports, players use aerodynamic effects to lure opponents and score. For example in soccer, a free kick may get around the defensive wall thanks to a side spin [1]. Among the different paths [2], one of the most intriguing paths is probably the zigzagging knuckleball. This rare event was first introduced in baseball by the Major League Baseball pitcher E Cicotte, in 1908 [3]. By mastering this pitch, Cicotte deserved the nickname ' Knuckles ' and finished his career with more than 200 wins [4]. After Cicotte, several pitchers mastered knuckleballs and the pitch became a nightmare for batters. Despite this old history, the scientific observation of zigzag paths on a baseball pitch has only been done recently by Nathan *et al* [5]. In this article, the authors measured the angular direction of pitches as observed by the batter as a function of the ball releasing speed for a 'normal' pitcher and a pitcher mastering knuckleballs. Nathan *et al* observe that the 'normal' pitcher Jon Lester is able to send the baseball with different techniques characterized by a precise releasing speed and a precise angular direction. This feature is different from the one observed with Tim Wakefield, famous for his knuckleballs. In his case, the ball is launched at a precise speed of 66 mph ($\simeq 29.5$ m s^{-1}) and follows a random angular direction characteristic of the knuckle effect. The releasing speed of knuckleballs is far below the maximal launching speed of baseballs observed in the field (105 mph $\simeq 47$ m s^{-1}). Nathan also determined that lateral deviations of knuckleballs are smaller than 1.2 cm which is 0.17 ball diameter [5]. Despite the slenderness of zigzag motions, the randomness of this pitch explains the difficulty for batters to hit them. Apart from baseball, zigzagging paths have been reported in volleyball and observed when the ball is launched with no spin [6]. Depra and co-workers measured these trajectories on a volleyball field and observed lateral deviations of the order of the ball diameter for a velocity of about 16 m s^{-1} [7]. Again, this velocity is far below the maximal velocity observed in volleyball, which is 37 m s^{-1}. Similar trajectories have finally been observed in soccer by Barber *et al* [8]. In this sport, zigzag paths occur with particular balls (such as the official match ball of the 2010 FIFA World Cup, *Jabulani*) when kicked with no spin [9]. Finally, knuckleballs have also been reported in cricket for a delivering speed of about 30 m s^{-1} [10].

We list in table 1 sports which involve balls of different diameters (4cm $\leqslant D \leqslant$ 24cm) and different velocities (10 m s^{-1} $\leqslant U_{\max} \leqslant$ 91 m s^{-1}). The corresponding Reynolds numbers ($Re = DU_{\max}/\nu$) based on the air viscosity ν are indicated in column 6 and observed to be in the range $3 \times 10^4 - 6 \times 10^5$. Despite the

Table 1. Characteristics of different ball games. Sports in which knuckleballs are observed are indicated in red (column 1). Ball diameter D (column 2) and mass M (column 3), ball to air density ratio ρ_b/ρ with $\rho = 1.2$ kg m^{-3} (column 4), maximal speed of the ball U_{max} recorded on sport fields (column 5), corresponding Reynolds number $Re = DU_{max}/\nu$ with ν the kinematic viscosity of air ($\nu = 1.5 \times 10^{-5}$ m s^{-2})(column 6). For sports where zigzag paths are reported (in red), the range of ball velocity U for which knuckleballs are obtained is reported in column 7 together with the typical length λ of a zigzag (column 8) and the range of normalized lateral deviation δ/D (column 9). Data are extracted from [2, 5–8, 11].

Sport	D (cm)	M (g)	ρ_b/ρ	U_{max} (m s^{-1})	$Re = DU_{max}/\nu$	U (m s^{-1})	λ (m)	δ/D
Table tennis	4	2.5	62	32	3×10^4	–	–	–
Bocce	8	700	2200	10	5×10^4	–	–	–
Tennis	6.5	55	318	73	1×10^5	–	–	–
Squash	4	24	597	78	1×10^5	–	–	–
Golf	4.2	45	967	91	2×10^5	–	–	–
Baseball	7.0	145	672	54	2×10^5	28–36	< 18	<0.3
Cricket	7.2	160	681	53	3×10^5	25–35	< 20	–
Volleyball	21	210	36	37	4×10^5	16–18	8–15	<1.5
Soccer	21	450	78	51	5×10^5	20–25	10–20	<1.5
Handball	19	450	104	27	6×10^5	–	–	–
Basketball	24	650	75	16	6×10^5	–	–	–

possible impact of aerodynamic forces in many of the sports listed in table 1 [2], knuckleballs are only reported for baseball, cricket, volleyball and soccer. Our goal is to understand why. The typical conditions and characteristics of zigzagging paths are gathered in the last columns of table 1. We notice that knuckleballs mostly occur in a narrow range of velocities (column 7), significantly below U_{max}, the maximum speed of each game (column 5). The typical length λ and amplitude δ of a zigzag are reported in the last two columns of table 1. Even if the lateral deviations δ are small, the unpredictability of this effect hinders receivers and goalkeepers. This phenomenon led one of the greatest baseball players, Willie Stargell, to describe knuckleballs as ' a butterfly with hiccups '.

The purpose of this paper is to identify a scenario able to account for these characteristics including the rareness of knuckleballs in sports. We first discuss the possible origins of the zigzags (section 2) including seams (section 2.1) and other sources of asymmetry (section 2.2). The experimental set-up able to produce knuckleballs is presented in section 3 together with the experimental results on zigzags. The equations of motion for sport balls are solved in section 4 taking into account unsteady lift forces. The different asymptotic regimes are discussed together with predictions of the mean lateral deviation and the typical wavelength of the zigzag path for various initial conditions (angles and velocities). We then propose a phase diagram in which sports where a knuckle effect may impact the game are identified (section 5).

2. Several possible origins

2.1. Effect of seams

A zigzag path is obtained provided a lateral unsteady asymmetry of the flow surrounding the ball exists. The first source of asymmetry considered to account for knuckleballs in baseball was the seams [12], a scenario recently revisited by Morissey *et al* [13].

Watts and Sayers measured the steady lift force in a wind tunnel for a baseball, as a function of its orientation θ with the flow (figure 1). They showed that lift oscillates with the ball orientation (figure 1(b)). Thus, when the ball slowly rotates in air, it undergoes an alternative lift, which leads to a zigzag path. The lateral deviations expected from this scenario can be estimated. We consider the ball motion along a direction z perpendicular to the baseball velocity $\boldsymbol{U}$ and to the gravitational acceleration $\boldsymbol{g}$ (figure 1(a)) and we assume along this direction a lift force $\boldsymbol{F}_L = F_{L,0} \sin(\omega t)\, \boldsymbol{e}_z$ with $\omega = 4\dot{\theta}$ (for a single rotation of the ball, the lift experiences about four oscillations due to the presence of four seams, as shown in figure 1(b)). The equation of motion of the ball projected along the z-direction is

$$M\frac{\mathrm{d}^2 z}{\mathrm{d}t^2} = F_{L,0} \sin(\omega t) \tag{1}$$

where $M = \pi\rho_b D^3/6$ is the mass of a ball of diameter D and density ρ_b. Equation (1) yields the lateral deviation of the ball

$$z(t) = -\frac{F_{L,0}}{M\omega^2} \sin(\omega t) \tag{2}$$

At $U = 20.7$ m s^{-1}, the measurements by Watts and Sayers provide $F_{L,0} \simeq 0.4$ N (figure 1(c)). In order to produce a complete zigzag on a distance λ corresponding to the distance between the pitcher and the batter

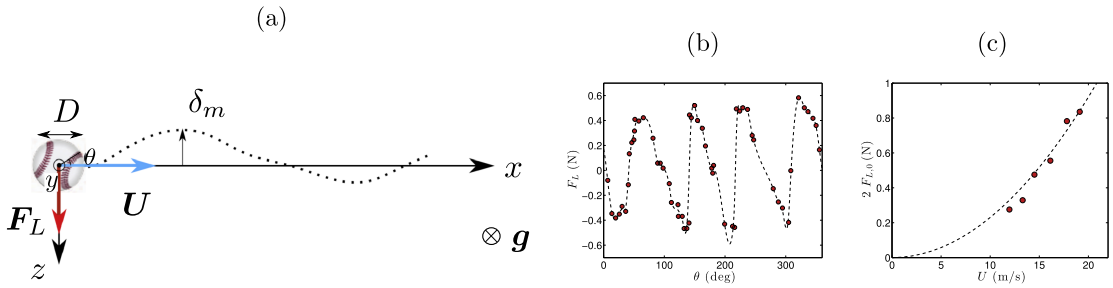

Figure 1. (a) Notations used to describe the deviation of a spinning baseball due to seams orientation. The axis of rotation is parallel to y and θ is the angle of a baseball ball symmetry plane relative to the velocity direction $\boldsymbol{U}$. This image has been obtained by the author from the Wikimedia website https://commons.wikimedia.org/wiki/File:Baseball.svg, where it is stated to have been released into the public domain. It is included within this article on that basis. (b) Lift force F_L as a function of the angle θ for $U = 20.7$ m s^{-1}. (c) Variation of the difference $2\,F_{L,0}$ between maximum and minimum lateral forces, as a function of the ball speed U. Data are extracted from [12].

($\lambda = 18.4$ m), the relation $\omega = 2\pi U/\lambda$ has to be satisfied and it yields $\dot{\theta} \simeq 1.8$ rad s^{-1}. In such a situation, the amplitude of the deviation is $\delta = F_{L,0}/M\omega^2$ which gives $\delta \simeq 0.4/0.145 \times 7^2 \simeq 0.06$ m, on the order of the ball diameter. This scenario may explain the zigzag paths reported on the pitch. However, it does not predict why knuckleballs are observed in a narrow window of ball velocity significantly below the maximal velocity achievable in game (table 1). Indeed, a shot at $U_0 = U_{\max}$ will maximize $F_{L,0}$ and thus δ as determined by Watts and Sayers (figure 1(c)). In addition, knuckleballs were also reported for balls without seams, which suggests that another scenario could be at play to explain this phenomenon.

2.2. Other possible origins

Other sources of asymmetry can be considered to account for knuckleballs. The flow profile around a sphere depends on the Reynolds number. Two characteristic features are generally stressed in the flow past a sphere: first, the stagnation points where the flow stops; secondly, the separation points where the boundary layer separates from the sphere. These characteristic points are represented in figure 2 with blue and red dots respectively. The up-down asymmetry of stagnation or separation points relative to the flow direction indicates the existence of a lift. For a smooth sphere and Reynolds numbers lower than unity, the flow profile is symmetric (figure 2(a)) and the particle experiences no lift force. In this case, the stagnation points are located at the poles of the sphere and there is no separation of the flow from the solid. When $Re < 300$, a symmetric recirculation zone appears behind the sphere (figure 2(b)). In this case, the flow separates from the sphere close to the equator as symbolized by red dots. For $Re > 300$, the alternate vortex shedding breaks the up-down symmetry and generates unsteady lift forces (figure 2(c)) [14]. If the sphere spins, its rotation also breaks the flow lateral symmetry, displaces the stagnation points and induces a steady lift force referred as a Magnus effect (figure 2(d)) [15]. As considered previously, the presence of surface roughnesses (seams for example) delays the separation of the boundary layer, moves the separation points out from the equator and provokes a lateral force (figure 2(e)) [16]. Finally, at $Re \simeq 3 \times 10^5$, an intermediate value between 10^4 and 10^6 (table 1) the boundary layer transits from laminar to turbulent state and the separation point moves downstream [17]. In the drag crisis, intermittent reattachments of the boundary layer generate temporarily asymmetric situations as shown in figure 2(f). Among these different sources of asymmetry, we try to identify the one which is likely to produce knuckleballs with the characteristics displayed in table 1.

3. Experimental setup and results

3.1. Set-up

In order to launch a ball with a minimum amount of spin, we developed a kicking machine composed of an electric motor, a steel arm and a flat plate as presented in figures 3(a) and (b). The power of the DC motor is 400 W, the arm has a length of 1.2 m and the dimensions of the flat plate are 20×20 cm^2. The rotational speed of the motor and the initial position of the ball imposes the launching conditions of the ball (initial speed and angle). The ball is a light and smooth beach ball of diameter $D = 20$ cm, mass $M = 120$ g and density $\rho_b = 29$ kg m^{-3}. Our set-up allows to launch the ball with an initial velocity U_0 between 0 and 16 m s^{-1} and an initial angle θ_0 between 0° and 45°. Moreover, the kicking machine launched the ball with a very small amount of spin, less than a tenth of a rotation along the entire trajectories ($\omega < 0.5$ rad s^{-1}).

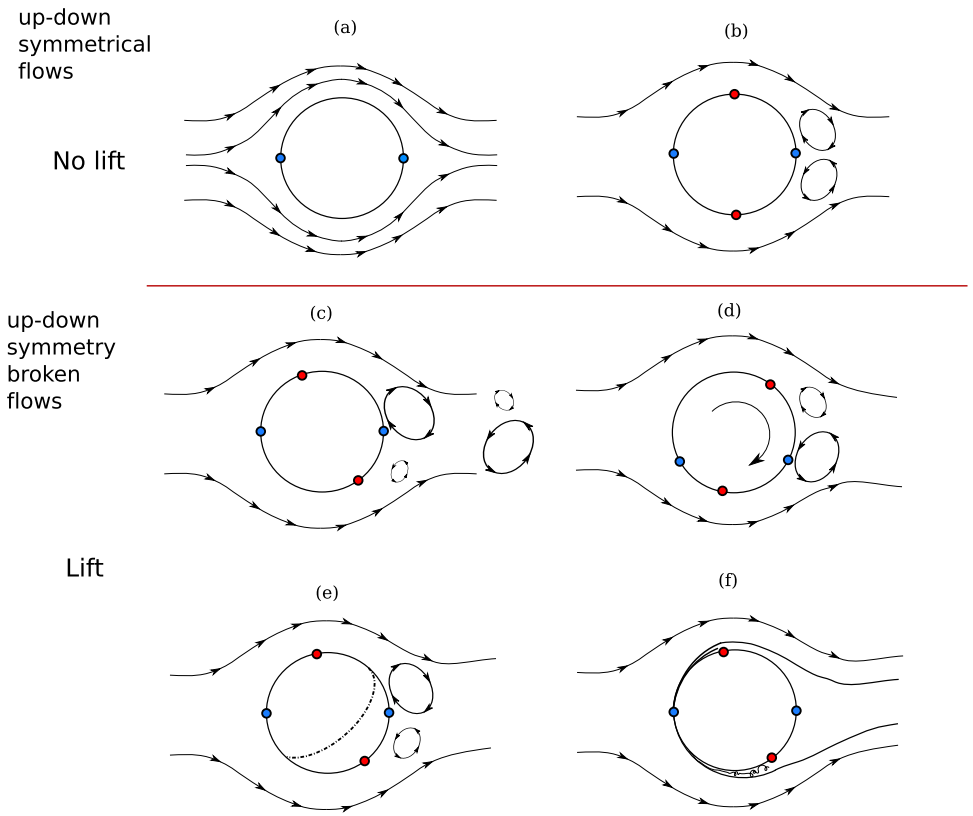

Figure 2. Sketch of the air flow surrounding a sphere at different Reynolds numbers and for various situations. Blue dots represent stagnation points whereas red dots represent separation points. (a) At low Reynolds number ($Re < 1$), the flow is symmetric. (b) For $1 < Re < 300$, a recirculation area exists behind the sphere, but the lateral symmetry is preserved. (c) For $Re > 300$, vortex shedding generates unsteady lift forces. (d) The sphere rotation breaks the flow lateral symmetry, which leads to a steady lift force known as the Magnus force. (e) The presence of a seam delays the boundary layer separation and gives a lift. (f) Asymmetry due to the boundary layer transition: the bottom layer is in a turbulent state whereas the upper one is still laminar.

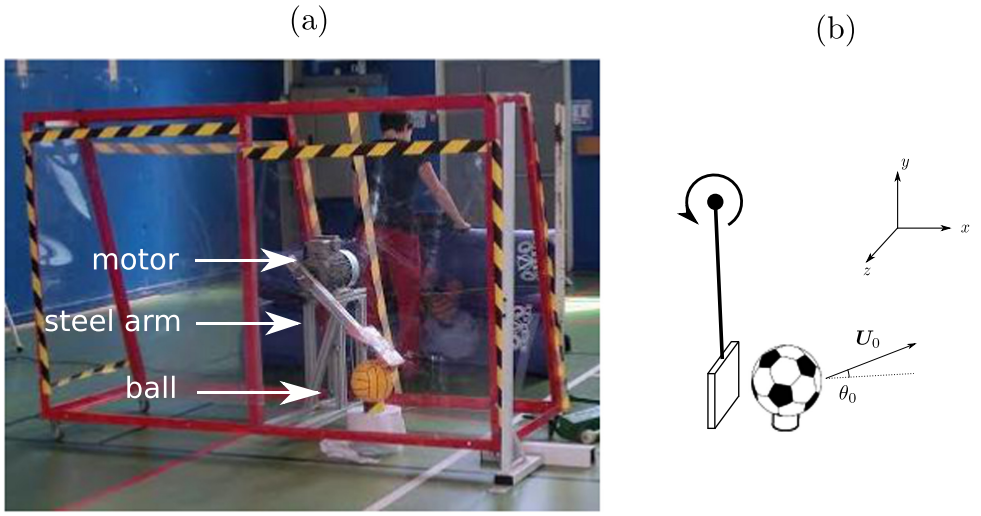

Figure 3. Image (a) and sketch (b) of the kicking machine used to shoot balls with no spin. This image has been obtained by the authors from the Wikimedia website https://commons.wikimedia.org/wiki/File:Soccerball.svg, where it is stated to have been released into the public domain. It is included within this article on that basis.

3.2. Experimental results

We recorded the motion of the ball with two high-speed cameras Photron SA3 looking from the front and from the side of the trajectory. The two cameras were synchronized with an external trigger and recorded the sequence at 1000 Hz in full resolution (1280 × 1024 pixels). Figure 4(a) shows the recorded trajectory from the side. One observes that the trajectory is slightly asymmetric with respect of the maximum, consistently with predictions of

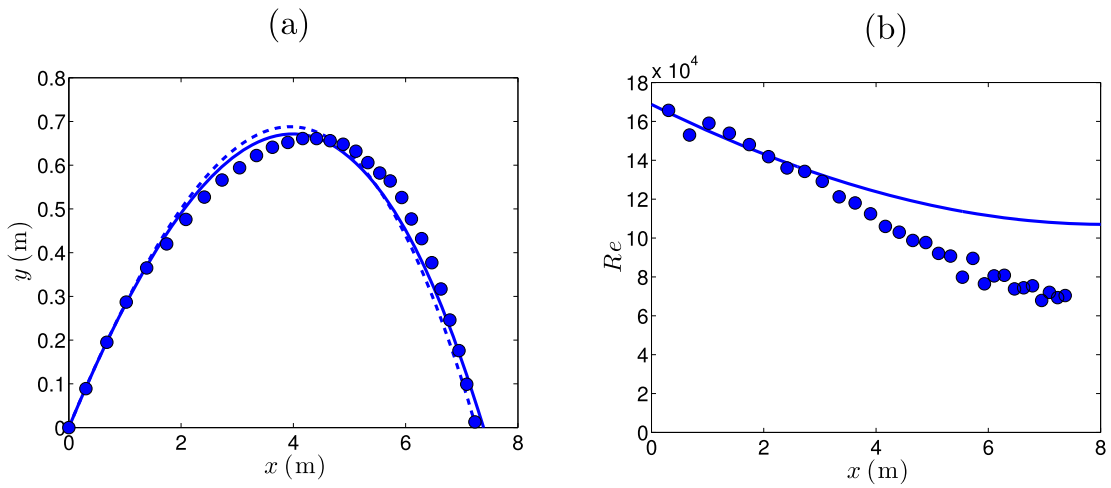

Figure 4. (a) Blue dots correspond to the side view of an experimental trajectory of a beach ball ($D = 20$ cm, $M = 120$ g and $\rho_b/\rho = 24$) launched with the initial conditions: $U_0 = 12$ m s^{-1}, $\theta_0 = 18°$ and no spin. the time interval between two ball positions is 24 ms. We estimate the terminal velocity of the ball $U_\infty = 12$ ms^{-1}, which leads to $U_0/U_\infty = 1$. Lines correspond to the numerical solutions of equations (3), (4) and (5) with $D = 20$ cm, $\rho_b/\rho = 24$ and $C_D = 0.4$ that is detailed in section 4. Initial launching conditions are the same as the experiment, $U_0 = 12$ m s^{-1}, $\theta_0 = 18°$ and $\psi_0 = 0°$. The dotted line shows the path of the ball without lift forces [$C_{L\,\theta}(t) = 0$ and $C_{L\,\psi}(t) = 0$] whereas the trajectory drawn with the solid line takes lift forces into account. (b) Blue dots represent the experiment Reynolds number $Re = DU/\nu$ of the flow around the ball as a function of its position along the x-direction. The time interval between two positions is 24 ms. The blue solid line corresponds to the numerical solution presented in section 4 with the same ball properties and initial conditions as the experiment ($D = 20$ cm, $\rho_b/\rho = 24$ and $C_D = 0.4$, $U_0 = 12$ m s^{-1}, $\theta_0 = 18°$ and $\psi_0 = 0°$).

Cohen *et al* [18] when the initial velocity of the ball U_0 is comparable to its free fall velocity U_∞ (in the present case $U_0/U_\infty \simeq 1.0$). From the side trajectory, we deduce the Reynolds number as a function of the horizontal distance x as shown in figure 4(b). The decrease of the Reynolds number along the trajectory is due to the drag which acts on the characteristic length $D\rho_b/\rho \sim 6$ m [18].

A front chronophotography of the ball till it reaches the top of the trajectory is shown in figure 5(a), revealing the non-straight path followed by the ball. Using the ball as a scale evolving over time, we deduced its lateral deviation along the z-direction as a function of the horizontal distance x and we report the data in figure 5(b). Initial conditions are similar, yet trajectories are different. This erratic behavior is the signature of knuckleballs. Lateral deviations of the ball are typically 0.1 to 0.4 ball diameter, that is, a few centimeters. Zigzags are observed on a traveled distance along the x-direction of about 7 m. Even if lateral deviations are small, they can strongly disturb volleyball receivers or soccer goalkeepers who are used to Magnus effect, but not to erratic phenomena.

4. Model

4.1. Equation of motion

The goal of this section is to solve the trajectory of a ball experiencing a drag $\boldsymbol{F}_D$ and an unsteady lift force $\boldsymbol{F}_L$ in addition to its weight $M\boldsymbol{g}$. At large Reynolds numbers the drag force is expressed as $\boldsymbol{F}_D = -\rho\pi\,(D/2)^2 C_D\, U\boldsymbol{U}/2$ with ρ the fluid density, D the ball diameter, $\boldsymbol{U}$ the ball velocity ($U = \|\boldsymbol{U}\|$) and C_D the drag coefficient. In this regime, the lift force is defined as $\boldsymbol{F}_L = \rho\pi\,(D/2)^2 U^2 (C_{L\,\theta}(t)\boldsymbol{e}_\theta + C_{L\,\psi}(t)\boldsymbol{e}_\psi)/2$ with $C_{L\,\theta}(t)$ and $C_{L\,\psi}(t)$ the instantaneous lift coefficients along $\boldsymbol{e}_\theta$ and $\boldsymbol{e}_\psi$, as defined in figure 6.

The equations of motion of the ball in the $(\boldsymbol{U}/U,\ \boldsymbol{e}_\theta,\ \boldsymbol{e}_\psi)$ frame are

$$\frac{\mathrm{d}U}{\mathrm{d}t} = -g\sin\theta - \frac{U^2}{\mathcal{L}} \tag{3}$$

$$\frac{\mathrm{d}\theta}{\mathrm{d}t} = -\frac{g\cos\theta}{U} + \frac{U}{\mathcal{L}_\theta} \tag{4}$$

$$\frac{\mathrm{d}\psi}{\mathrm{d}t} = \frac{U}{\mathcal{L}_\phi} \tag{5}$$

where $\mathcal{L} = 2M/\rho\pi\,(D/2)^2 C_D$, $\mathcal{L}_\theta = 2M/\rho\pi\,(D/2)^2 C_{L\theta}(t)$ and $\mathcal{L}_\phi = 2M/\rho\pi\,(D/2)^2 C_{L\phi}(t)$ are the characteristic lengths associated to drag and lift forces. Without lift, equations (3), (4) and (5) reduce to a 'Tartaglia' path [18]. In the general case, solving these equations requires to know the time evolution of the lift coefficients $C_{L\theta}(t)$ and $C_{L\,\psi}(t)$. Lift coefficients typically reported in the literature are time-averaged quantities. However, owning

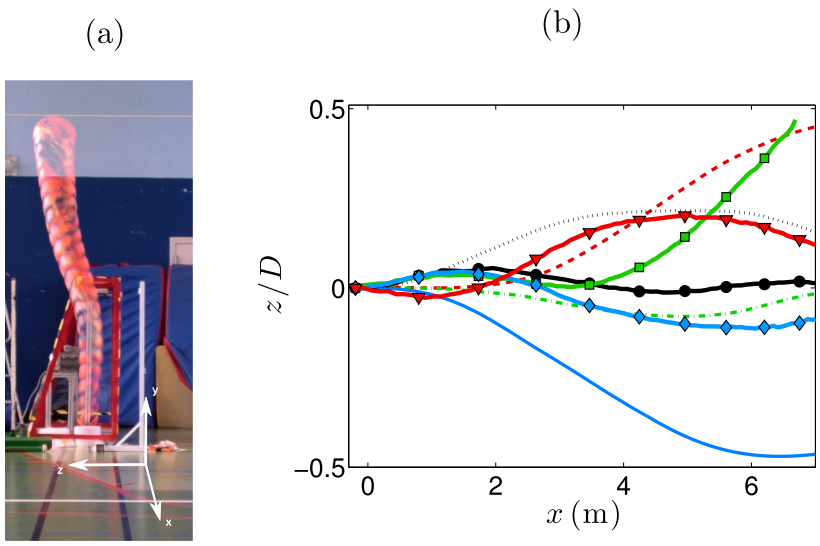

Figure 5. (a) Chronophotography of a beach ball launched with the kicking machine described in section 3.1. The camera faces the kicking machine and the time interval between two positions is 33 ms. For the sake of clarity, the chronophotography only shows the first part of the trajectory where the ball undergoes an upward motion. (b) Lines with symbols correspond to top view of experimental trajectories for a beach ball ($D = 20$ cm, $M = 120$ g and $\rho_b/\rho = 24$) launched four times with same initial conditions ($U_0 = 12$ m s^{-1}, $\theta_0 = 18°$ and no spin). Lines without symbols represent the numerical solutions of the model presented in section 4 for same ball properties and initial conditions as in the experiment. The difference between the four numerical trajectories arises from the choice of the phase Ψ in the lift coefficient decomposition.

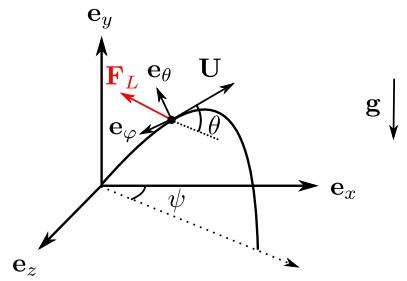

Figure 6. Conventions used in the trajectory calculation.

to the complex time-dependent interactions in the boundary layer, the real lift coefficients are not constant in time. Rather than solving the turbulent fluid equation in the boundary layer, we propose to use an effective time-dependent lift coefficient that mirrors this measured spectrum. From experimental data presented in figure 5(b), we evaluate the characteristic time of a deviation as $\lambda/U \simeq 8/16 = 0.5$ s where $\lambda \sim 8$ m is the typical wavelength of a zigzag. This time is long compared to the convective time $D/U \simeq 0.2/16 \simeq 10$ ms. For the flow, the lateral motion of the ball is thus quasi-steady. We thus use the spectrum of lift force fluctuations measured using wind tunnel tests in order to solve the equations of motion. Norman and McKeon reported the spectral density Φ of the lift as a function of the dimensionless frequency $St = fD/U$ (also known as Strouhal number) and the Reynolds number for a smooth sphere in the sub-critical, critical and super-critical regimes [19]. Examples of these measurements are shown in figures 7(a) and (b). These data allow us to express the instantaneous lift coefficients by the way of a Fourier decomposition

$$C_L(t) = \int_0^\infty \tilde{C}_L(f) \sin(2\pi f t + \Psi)\, \mathrm{d}f \tag{6}$$

where $\tilde{C}_L = \sqrt{\Phi}$ and Ψ are the amplitude and phase of each spectral component that possibly depend on Strouhal and Reynolds numbers.

4.2. Comparison of the numerical trajectories with the experiments

We now solve numerically the equations of motion introduced in the previous section. The properties of the ball considered for the numerical method are the same as in section 3 ($D = 20$ cm, $\rho_b/\rho = 30$ and $C_D = 0.4$) in

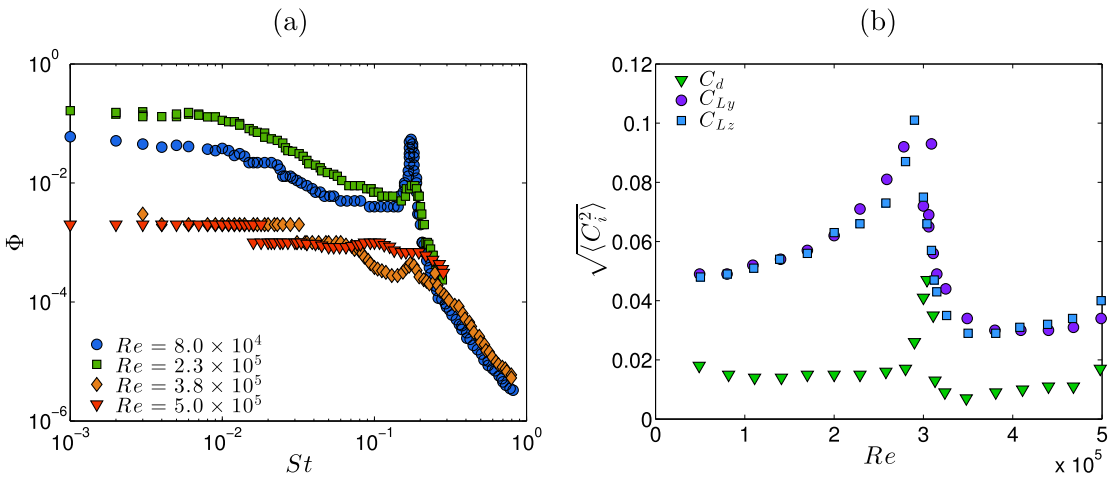

Figure 7. (a) Normalized spectral power density Φ of lift forces as a function of the Strouhal number $St = fD/U$ measured by Norman and McKeon for a smooth sphere [19]. Blue dots correspond to $Re = 8.0 \times 10^4$, green squares to $Re = 2.3 \times 10^5$, orange diamonds to $Re = 3.8 \times 10^5$ and red triangles to $Re = 5.0 \times 10^5$. (b) Variance over time of the drag coefficient (green triangles) and lift coefficients along the two transverse directions y and z (respectively purple dots and blue squares) as a function of the Reynolds number. Data are extracted from [19].

order to compare numerics with experiments. Concerning the numerical method, we first solve equations (3), (4) and (5) without lift in order to determine the evolution of the Reynolds number along the trajectory. Then, we include fluctuating lift forces associated to the local Reynolds number as measured by Norman and McKeon with equation (6) [19]. Note that as the phase Ψ of each spectral component was not reported, we choose this parameter randomly. Such a choice made each solution unique but does not impact, statistically, the zigzagging phenomenon. Figures 4(a) and 5(b) show a side view and a top view of the numerical trajectories.

One observes in figure 4(a) that lift forces have little impact on the overall ball trajectory (plane (O, x, y)) but a visible effect in the (O, x, z) plane (figure 5(b)). By performing several numerical simulations with the same initial conditions, we estimate the mean lateral amplitude and the typical wavelength of the zigzag. Lateral deviations are about 0.3 ball diameter and zigzag occurs on a distance of about 8 m, which is of the same order of magnitude as the experimental observations described in section 3. In conclusion, the wind tunnel measurements of unsteady lift made by Norman and McKeon for a smooth sphere lead to a qualitative agreement with observations of the trajectories of free moving spheres.

However, the numerical reproduction of zigzag trajectories does not allow us to make any prediction on the moment they occur, or why we only observe them in a few sports. In order to understand more deeply what provokes knuckleballs, we consider below the different contributions of the lift force spectrum separately. Indeed, we observe in figure 7(a) that the spectral density Φ of the lift force for $Re < 3 \times 10^5$ exhibits three distinct features: a white noise behavior in the range $St < 0.1$, a peak at $St \simeq 0.2$ which corresponds to vortex shedding [14] and a power law decrease at large Strouhal numbers ($St > 0.3$). For $Re > 3 \times 10^5$, the peak corresponding to vortex shedding disappears but both the low frequency white noise and the large frequency decrease remain (figure 7(b)).

4.3. The vortex shedding limit

For the sake of clarity, the impact of vortex shedding on the trajectory is considered in the naive case where the ball moves at a constant velocity $\boldsymbol{U} = U\ \boldsymbol{e}_x$ with only a lift force along the z-direction. In such a situation, the equations of motion (3), (4) and (5) reduce to

$$\frac{\mathrm{d}^2 z}{\mathrm{d}t^2} = \frac{3}{4}\frac{\rho}{\rho_b}\frac{U^2}{D} C_L(t) \tag{7}$$

where $\rho_b = M/(\pi D^3/6)$ is the ball density. Assuming that the spectrum of lift is a single peak for $St \simeq 0.2$, equation (6) becomes

$$C_L(t) = \tilde{C}_L \sin(2\pi f t) \tag{8}$$

with $f = 0.2\ U/D$ and $\tilde{C}_L = \tilde{C}_L(St = 0.2)$. In this context, the equation of motion (7) yields

$$\frac{\mathrm{d}^2 z}{\mathrm{d}t^2} = \frac{3}{4}\frac{\rho}{\rho_b}\frac{U^2}{D}\tilde{C}_L \sin(2\pi f t) \tag{9}$$

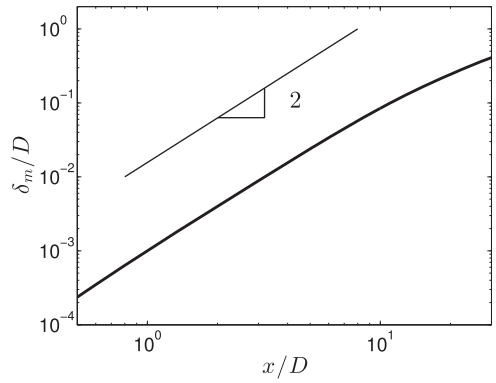

Figure 8. Mean normalized lateral deviation δ_m/D of the trajectory along the z-direction as a function of the normalized traveled distance x/D. The plot results from the solution of equations (3), (4) and (5) with $D = 20$ cm, $\rho_b/\rho = 24$ and $C_D = 0.4$ and initial conditions $U_0 = 12\ \mathrm{m\,s^{-1}}$, $\theta_0 = 18°$ and $\psi_0 = 0°$. A mean over N = 1000 trajectories is calculated in order to get this plot thanks to the expression $\delta_m(\boldsymbol{r}_0) = \frac{1}{N}\sum_{i=1}^{N}\sqrt{(\boldsymbol{r}_i - \boldsymbol{r}_0)^2}$ where $\boldsymbol{r}_i$ and $\boldsymbol{r}_0$ are the positions of the ball if lift forces are considered or not.

The amplitude δ of the zigzag along the z-direction can be deduced to be

$$\frac{\delta}{D} = \frac{3}{16\pi^2}\frac{\rho}{\rho_b}\frac{\tilde{C}_L}{St^2} \tag{10}$$

The normalized lateral deviation δ/D produced by vortex shedding at $St \simeq 0.2$ depends on the inverse of the ball-air density ratio ρ_b/ρ. Horowitz and Williamson proved that for light spheres ($\rho_b/\rho < 1$), this phenomenon provokes alternate deviations of about a ball diameter [20]. A review of rising and falling non-rectilinear trajectories of a sphere in a fluid was proposed by Ern *et al* [21]. In sports, the ratio ρ_b/ρ is much larger than unity ($46 < \rho_b/\rho < 570$, see table 1), so that we expect negligible lateral deviations ($\delta/D \ll 1$). In conclusion, the classical vortex shedding is not responsible for knuckleballs.

4.4. The white noise limit

In this section, we consider the low frequency limit of the spectrum of lift force, which is close to a white noise (figures 7(a) and (b)). As in section 4.3, each frequency f in the lift force is associated to a normalized maximal deviation

$$\frac{\delta}{D} = \frac{3}{16\pi^2}\frac{\rho}{\rho_b}\tilde{C}_L\left(\frac{U}{fD}\right)^2 \tag{11}$$

For a traveled distance x, the minimal frequency corresponding to a complete zigzag is $f = U/x$; combining it with equation (11), we get

$$\frac{\delta}{D} = \frac{3}{16\pi^2}\frac{\rho}{\rho_b}\tilde{C}_L\left(\frac{x}{D}\right)^2 \tag{12}$$

The lateral deviation δ still depends on the inverse of the density ratio ρ_b/ρ and on the lift coefficient $\tilde{C}_L$ but it is also a function of the distance x over which balls are observed: the larger x, the larger the lateral deviations, in agreement with what can be observed in figure 5(b). This behavior is verified more quantitatively in figure 8 where the mean lateral deviation δ_m is presented as a function of the ball position along the x-axis. The quantity δ_m is calculated over $N = 1000$ trajectories obtained with numerical methods presented in section 4.1 by the way of the relation: $\delta_m(\boldsymbol{r}_0) = \frac{1}{N}\sum_{i=1}^{N}\sqrt{(\boldsymbol{r}_i - \boldsymbol{r}_0)^2}$ where $\boldsymbol{r}_i$ and $\boldsymbol{r}_0$ are the positions of the ball if lift forces are considered or not. One notices in figure 8 the square dependence of δ_m/D on x/D predicted by relation (12). Hence, we expect lateral deviations to become significant only if the trajectory is long enough, so that field size and gravity are limiting factors for the observation of zigzags. Moreover, Norman and McKeon reported that the value of the lift coefficient $\tilde{C}_L$ at low frequency ($St < 0.1$) has a non-trivial variation with the Reynolds number (figure 7(c)). The variance of lift coefficients over time $\sqrt{\langle C_L^2(t)\rangle}$ shows a maximum close to $Re \simeq 3 \times 10^5$ which corresponds to the drag crisis regime. The intermittent reattachment of the boundary layer is responsible for this effect [19]. Thereby, if a ball is launched in the range of velocity corresponding to the drag crisis ($Re \simeq 3 \times 10^5$ for a smooth sphere), we expect lateral deviations to be increased.

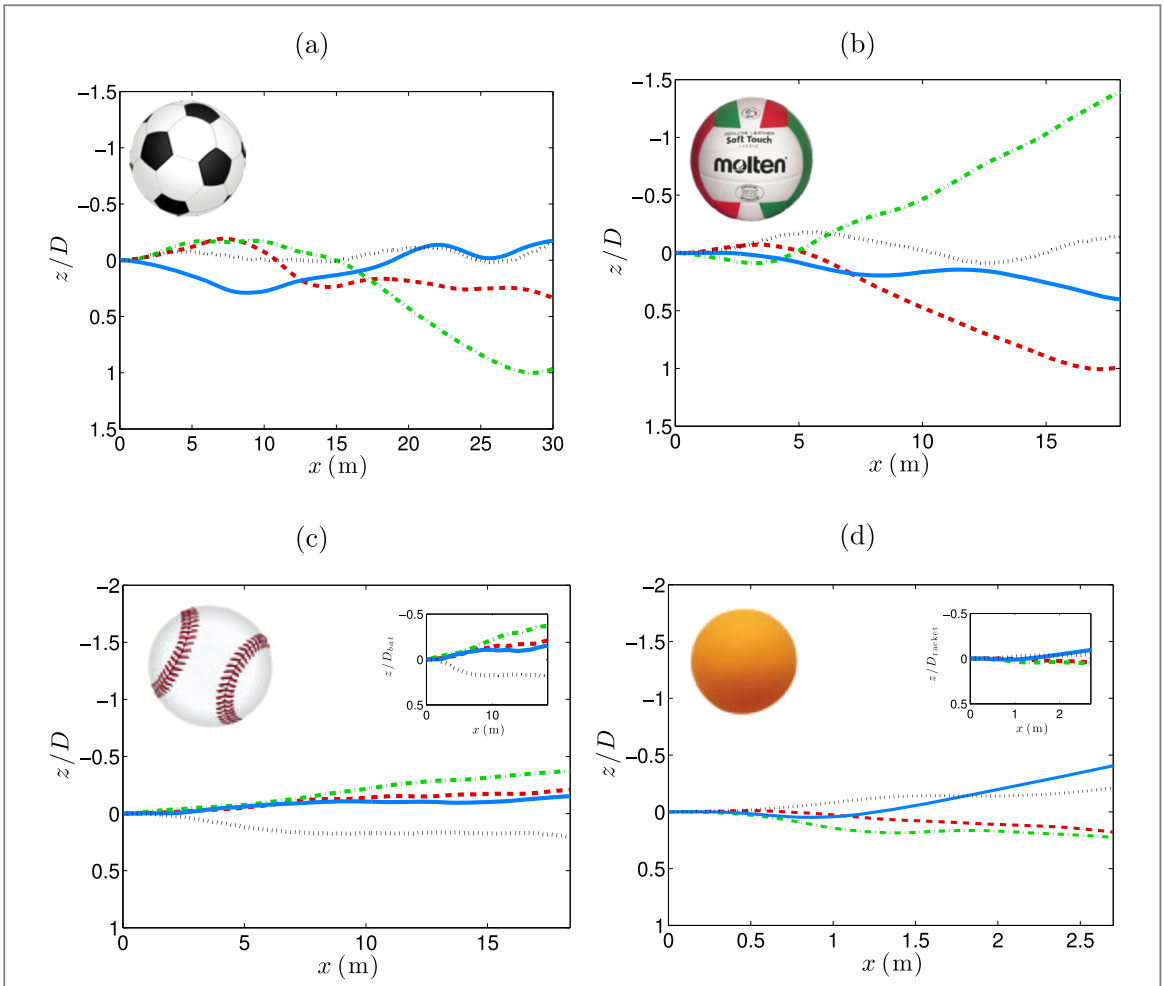

Figure 9. Numerical trajectories computed with equations (3), (4) and (5) for different sports balls. The trajectories are projected in the (x, z) plane, which corresponds to a top view. In each case, four trajectories are computed with the same set of parameters and initial conditions. (a) Soccer ball: $D = 21$ cm, $\rho_b/\rho = 78$ and $C_D = 0.24$. Initial conditions are $U_0 = 25$ m s^{-1}, $\theta_0 = 5°$ and $\psi_0 = 0°$. This image has been obtained by the authors from https://pixabay.com/fr/soccer-boule-le-sport-jeu-l-équipe-34898/, where it is stated to have been released into the public domain. It is included within this article on that basis. (b) Volleyball: $D = 21$ cm, $\rho_b/\rho = 36$ and $C_D = 0.25$. Initial conditions are $U_0 = 18$ m s^{-1}, $\theta_0 = 20°$ and $\psi_0 = 0°$. This image has been obtained by the authors from the Wikimedia website https://commons.wikimedia.org/wiki/File:Volleyball.jpg, where it is stated to have been released into the public domain. It is included within this article on that basis. (c) Baseball ball: $D = 7.0$ cm, $\rho_b/\rho = 672$ and $C_D = 0.38$. Initial conditions are $U_0 = 30$ m s^{-1}, $\theta_0 = 5°$ and $\psi_0 = 0°$. The inset shows the same trajectories with the lateral deviations normalized by the diameter of the bat ($D_{\text{bat}} = 7$ cm). This image has been obtained by the authors from the Wikimedia website https://commons.wikimedia.org/wiki/File:Baseball.svg, where it is stated to have been released into the public domain. It is included within this article on that basis. (d) Table tennis ball: $D = 4.0$ cm, $\rho_b/\rho = 62$ and $C_D = 0.36$. Initial conditions are $U_0 = 30$ m s^{-1}, $\theta_0 = 0°$ and $\psi_0 = 0°$. The inset shows the same trajectories with the lateral deviations normalized by the diameter of the racket (D_{racket}=17 cm). This image has been obtained by the authors from the Wikimedia website https://commons.wikimedia.org/wiki/File:Table_tennis_ball.png, where it is stated to have been released into the public domain. It is included within this article on that basis.

5. Knuckleballs in sports

5.1. Numerical trajectories

The numerical integration of the equations of motion (3), (4) and (5) is done for the ball properties listed in table 1. Figure 9 shows the numerical results in the (O, x, z) plane (top view) for soccer, volleyball, baseball and table tennis. In each situation, the numerical method has been driven four times with a different choice in the spectral phase Ψ, which allows us to appreciate the mean lateral deviation produced by the lift forces and the typical zigzagging wavelength.

For a soccer ball (figure 9(a)), lateral deviations are about a ball diameter after 30 m. Between one and two changes in transverse direction are observed. Compared to soccer, lateral deviations are increased for a volleyball while wavelengths are reduced (figure 9(b)). On the distance which separates the batter and the pitcher in baseball, balls have about one change in lateral direction and typical excursions are about 0.5 ball diameter (about 3 cm) (figure 9(c)). The predictions show qualitative agreement with observations of knuckleballs in the field (see table 1), which confirms that the unsteady lift experienced by a sphere can be responsible for knuckleballs. Numerical solutions for a table tennis ball exhibit transverse deviations lower than 0.5 ball

Table 2. Characteristics of knuckle trajectories deduced from the numerical method presented in section 4 (column 1): ball diameter D (column 2), solid-air density ratio ρ_b/ρ (column 3), typical length L_{shot} from which a shot is performed to score (column 4), ball velocity U_{shot} for which the zigzag effect is larger ($\delta = \delta_{\max}$) (column 5), zigzag wavelength $\lambda = 2\pi D\sqrt{4\rho_b/3\rho}$ (column 6), ratio between the typical shot distance and the wavelength L_{shot}/λ (column 7) and maximal normalized mean deviation $\delta_{\max}/D$ in the range of Reynolds number encountered in the game and for a traveled distance corresponding to λ (column 8), ratio between the characteristics time of a zigzag and the reaction time $\tau_{\text{knuckle}}/\tau = \lambda/U_{\text{shot}}\tau$ (column 9). Sports highlighted in red are those where knuckleballs are expected to be observed according to our model.

Sport	D (cm)	ρ_b/ρ	L_{shot} (m)	U_{shot} (m s^{-1})	λ (m)	L_{shot}/λ	$\delta_{\max}/D$	$\tau_{\text{knuckle}}/\tau$
Table tennis	4.0	62	3	32	2.3	1.2	0.5	0.07
Bocce	8.0	2200	15	10	27	0.5	0.01	2.7
Tennis	6.5	318	24	73	8	3.0	0.3	0.11
Squash	4	597	10	78	7	1.4	0.2	0.09
Golf	4.2	967	100	91	9.5	10.6	1.2	0.10
Baseball	7.0	672	18.4	54	13.1	1.4	0.8	0.24
Cricket	7.2	681	20	53	13.6	1.5	0.6	0.26
Volleyball	21	36	18	28	9.1	2.0	2.5	0.33
Soccer	21	78	30	20	13.5	2.2	1.7	0.70
Handball	19	104	6	13	14	0.4	0.3	1.1
Basketball	24	75	8	8	15	0.5	0.1	1.9

diameter over a distance corresponding to the table length (figure 9(d)). Baseball and table tennis have about the same amplitude of lateral deviations. However if these deviations are compared with the dimensions of the sweet spot of bats and table tennis rackets [22, 23], one can infer that zigzagging balls are more difficult to catch in baseball than in table tennis (see insets in figures 9(c) and (d) where the lateral deviations are normalized by the bat or racket diameter).

5.2. Conditions for observation

As knuckleballs are not observed in all sports, we finally discuss the conditions to observe zigzags. Assuming that this phenomenon comes from the white noise present in the spectrum of lift forces described in section 4.4, we use equation (12) for the prediction of the lateral deviation δ of a ball which has followed a zigzag motion by a distance x. The equation can be written in the following way

$$\frac{\delta}{D} = \tilde{C}_L\left(\frac{x}{\lambda}\right)^2 \tag{13}$$

where $\lambda = 2\pi D\sqrt{4\rho_b/3\rho}$ is a typical distance fixed by the ball diameter D and the solid-fluid density ratio ρ_b/ρ and reported for the different sports in table 2. One deduces from equation (13) that zigzag with a significant lateral deviation ($\delta > D$) requires trajectories longer than λ. However, the distance traveled by the ball is not the only criterion needed to observe a tortuous path. Indeed, equation (13) shows that the spectral intensity $\tilde{C}_L$ must be large enough in order to produce a significant deviation. More precisely, it is the spectral intensity of lift components of frequencies lower than $f = U/\lambda$ that is important. The two conditions are discussed in what follows.

The criteria for long trajectories can be approached by comparing the minimal zigzag wavelength λ to the typical distance L_{shot} from which the different sport balls are shot to score. The distances λ and L_{shot} and their ratio are reported in table 2. For sports where $L_{\text{shot}}/\lambda > 1$, it will be possible to observe a complete zigzag and most sports (except bocce, handball and basketball) satisfy this criterion.

As for the spectral intensity $\tilde{C}_L$ of lift forces at low frequency ($f < \lambda/U$), Norman and McKeon showed that $\tilde{C}_L$ reaches a maximum for $Re \simeq 3 \times 10^5$ (figure 7(c)). Thereby, the ball velocity will impact non-trivially the zigzag properties and we try here to estimate how. We study numerically the effect of the initial velocity of the ball U_0 on the mean lateral deviation δ_m respectively to the trajectory expected without lift. The quantity δ_m is calculated over $N = 1000$ trajectories obtained from numerical solutions of equations (3), (4) and (5) with the procedure described in section 4.4. Figure 10(a) shows the evolution of the mean normalized lateral deviation δ_m/D for a ball having the characteristics of a soccer ball ($D = 21$ cm, $\rho_b/\rho = 90$ and $C_D = 0.23$) as a function of the initial Reynolds number $Re_0 = DU_0/\nu$. The ratio δ_m/D is estimated for different distances traveled by the ball along the x-direction.

As seen in figure 10(a), δ_m increases with the traveled distance x as expected from equation (12). The evolution of δ_m with Re_0 is non-monotonic and it reaches a maximum for $Re \simeq 3.0 \times 10^5$. This observation directly results from the fact that fluctuations of the lift coefficients reach a maximum at the drag crisis (figure 7(c)). We evidenced the asymmetry of the flow past a sphere in the drag crisis with an experiment achieved in the wind tunnel of the LME laboratory in Valenciennes. We measure the angle θ_w of the wake past a

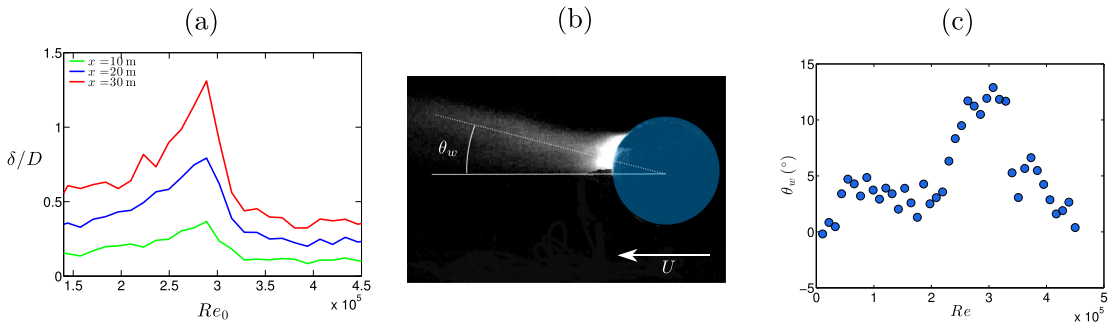

Figure 10. (a) Mean normalized lateral deviations δ_m/D of a soccer ball trajectory compared with the trajectory expected without lift forces, as a function of the initial Reynolds number $Re_0 = DU_0/\nu$ for various traveled distances along the x-direction. The quantity δ_m is derived by solving equations (3), (4) and (5) and using the definition $\delta(\boldsymbol{r}_0) = \frac{1}{N}\sum_{i=1}^{N}\sqrt{(\boldsymbol{r}_i - \boldsymbol{r}_0)^2}$ with $N = 1000$. The ball characteristics correspond to the one of a soccer ball: $D = 21$ cm, $\rho_b/\rho = 90$ and $C_D = 0.23$. (b) Picture of the experiment made in a wind tunnel. A smooth sphere of diameter $D = 30$ cm is placed in an air flow and the injection of smoke at the rear of the sphere allows us to visualize the mean direction of its wake θ_w relatively to the direction of the air flow. (c) Angle θ_w of the wake as a function of the Reynolds number.

smooth sphere relatively with the direction of the flow $\boldsymbol{U}$ (defined in figure 10(b)) as a function of the Reynolds number. One observes in figure 10(c) that the asymmetry in the wake dramatically increases when $Re \sim 3 \times 10^5$. Thereby, the knuckle effect of a non-spinning ball is enhanced if the range of initial velocity corresponds to the drag crisis. One knows that the critical Reynolds number of the drag crisis strongly depends on the texture of the ball [24]. This effect occurs in a range of velocity between 15 m s^{-1} and 25 m s^{-1} for soccer [25], between 16 m s^{-1} and 18 m s^{-1} for volleyball [6] and between 30 and 35 m s^{-1} for baseball [16]. All these ranges of velocity are in good agreement with the ones where knuckleballs are observed [table 1]: increase of lateral deviations in the drag crisis regime appears to be essential to observe zigzag paths in sports.

5.3. Phase diagram for knuckleballs

The minimal flight length and the speed required to observe a knuckle effect in sport can be summarized in a phase diagram. We reported in table 2 the maximal normalized deviation $\delta_{\max}/D$ experienced when the projectile has traveled by a distance λ from its releasing point. The quantity $\delta_{\max}$ is the maximal value of the mean deviation of the ball δ_m in the range of Reynolds number encountered in the considered sport (see table 1). One notices that $\delta_{\max}/D$ is lower than 0.5 in bocce, handball, basketball, squash, tennis and table tennis. For such balls, a zigzag path never disturbs players. The two criteria to obtain a knuckle effect are gathered in figure 11, where the coordinates are the ratios $\delta_{\max}/D$ and L_{shot}/λ for each sport.

In this plot, sports where knuckleballs may perturb the game are located in the domain where $L_{\text{shot}}/\lambda > 1$ and $\delta_{\max}/D > 1$. In the others domains of the diagram, knuckleballs cannot be observed, either because of small transverse deviations or because wavelengths are longer than the field. For sports producing knuckleballs, it is required to launch the ball at very low spin and in the good range of initial velocities. These conditions may be difficult to obtain, especially in sports where the time of execution of a technical movement has to be minimized. Also, one may guess that it will be easier to launch a ball without spin by kicking it with a flat surface such as a racket rather than with a curved surface such as a bat. Despite that the link between the shape of the impactor and the easiness to produce knuckleballs is out of the scoop of this study, one may think that zigzag trajectories are simpler to produce in volleyball than in baseball for such a reason.

Surprisingly, golf balls belong to sports where knuckleballs may occur while no study reports such a behavior. Several arguments can be advanced to explain this enigma: first golf balls always experience a large spin, which produces a Magnus lift force much larger than the lift force unsteadiness discussed in this paper; secondly the resolution of the human vision does not allow to distinguish the lateral motion of the ball at a large distance; and of course there is no catcher in golf to be disturbed by a zigzag flight.

5.4. Characteristic time

So far, the characteristics time over which knuckleballs occur have not been discussed. Such a time can be estimated as $\tau_{\text{knuckle}} = \lambda/U_{\text{shot}}$ and compared with the typical reaction time of a player $\tau \simeq 1$ s as introduced earlier by Darbois Texier *et al* [11]. One expects that if $\tau_{\text{knuckle}} > \tau$, players can react to ball motions and catch zigzagging paths. On the contrary, if the reaction time τ is longer than the characteristics zigzagging time τ_{knuckle}, knuckleballs can lure players. The ratio of the two characteristics times $\tau_{\text{knuckle}}/\tau$ is reported in the last column of table 2. One notices that in all sports where knuckle effect plays a role, the ratio $\tau_{\text{knuckle}}/\tau$ is smaller than one. Such an observation implies that in sports where zigzag paths can be observed, they systematically disturb the

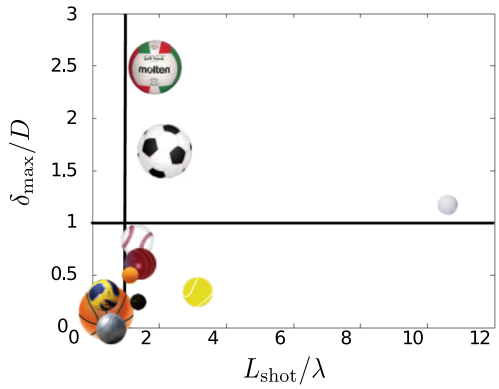

Figure 11. Maximal normalized mean lateral deviation $\delta_{\max}/D$ observed in each sport as a function of the ratio of field length L_{shot} and zigzag wavelength λ. Data are obtained from the two final columns of table 2. Golf ball: this image has been obtained by the authors from www.publicdomainpictures.net/view-image.php?image=36592&picture=golf-ball, where it is stated to have been released into the public domain. It is included within this article on that basis. Tennis ball: this image has been obtained by the authors from the Wikimedia website https://commons.wikimedia.org/wiki/File:Tennis_ball_3.svg, where it is stated to have been released into the public domain. It is included within this article on that basis. Bocce ball: this image has been obtained by the authors from https://pixabay.com/fr/pétanque-boule-sport-jouer-boules-381155/, where it is stated to have been released into the public domain. It is included within this article on that basis. Cricket ball: this image has been obtained by the author from https://pixabay.com/fr/balle-de-cricket-cricket-boule-295206/, where it is stated to have been released into the public domain. It is included within this article on that basis. Squash ball: this image has been obtained by the authors from the Wikimedia website https://commons.wikimedia.org/wiki/File:Squash_Ball_Dunlop_Revelation_Pro_2.jpg, where it is stated to have been released into the public domain. It is included within this article on that basis. Basketball: this image has been obtained by the author from the Wikimedia website https://commons.wikimedia.org/wiki/File:Basketball_Ball_Icon.png, where it is stated to have been released into the public domain. It is included within this article on that basis. Handball: this image has been obtained by the authors from the Wikimedia website https://commons.wikimedia.org/wiki/File:Handball_the_ball2.png, where it is stated to have been released into the public domain. It is included within this article on that basis. Soccer ball: this image has been obtained by the authors from https://pixabay.com/fr/soccer-boule-le-sport-jeu-l-équipe-34898/, where it is stated to have been released into the public domain. It is included within this article on that basis. Volleyball: this image has been obtained by the authors from the Wikimedia website https://commons.wikimedia.org/wiki/File:Volleyball.jpg, where it is stated to have been released into the public domain. It is included within this article on that basis. Baseball: this image has been obtained by the authors from the Wikimedia website https://commons.wikimedia.org/wiki/File:Baseball.svg, where it is stated to have been released into the public domain. It is included within this article on that basis. Table tennis ball: this image has been obtained by the authors from the Wikimedia website https://commons.wikimedia.org/wiki/File:Table_tennis_ball.png, where it is stated to have been released into the public domain. It is included within this article on that basis.

game. More particularly, one remarks that the ratio of the zigzagging time over the reaction time is smaller in baseball than in volleyball and soccer. Catching a knuckleball in baseball requires shorter reflexes than in volleyball and soccer and may explain why such phenomenon were first reported in baseball.

Conclusion

We have considered different possible origins for knuckleballs. These zigzag trajectories are associated to asymmetric and unsteady flows of air around the ball. We first quantified zigzags with an experiment, and then modeled them theoretically. Using unsteady lift forces, we obtain a quasi-quantitative agreement with experimental trajectories of a non-spinning ball traveling through the air. Using the numerical integration, we estimated the lateral deviations and the wavelengths expected for each sport ball, and predict how the unsteadiness of lift forces can produce a change in lateral directions within a field and with a sufficient magnitude to disturb players. In these sports, we showed that the obtention of a large knuckle effect requires the ball to be launched in a particular range of initial velocities corresponding to the drag crisis of the ball. This criterion, plus the absence of initial spin, explains the rareness of knuckleballs in sport. It also explain why the effect is only observed in a narrow range of ball velocities.

In baseball, the proposed scenario and the one involving the seams are both compatible. Knuckleballs in this sport may thus have two different origins, keeping their complexity veiled and remaining a nightmare for batters.

Acknowledgments

Caroline Frot and Antoine Garcia are thanked for their precious help in the realization of a safe kicking machine. We acknowledge Dominique Legendre for performing numerical simulations which guide us in this work. Also,

we thank Francois Gallaire, Lloyd Smith and Alan Nathan for many relevant discussions. Finally, the authors acknowledge Fawaz Massouh and Ivan Dobrev for providing us the access to the wind tunnel of the ENSAM school and Laurent Keirsbulck for the access to the wind tunnel of the LME laboratory which both give us experimental confirmations of the previous scenario.

References

[1] Dupeux G, Le Goff A, Quéré D and Clanet C 2010 The spinning ball spiral *New J. Phys.* **12** 093004
[2] Clanet C 2015 Sports ballistics *Ann. Rev. Fluid Mechanics* **47** 455–78
[3] Borg J P and Morrissey M P 2014 Aerodynamics of the knuckleball pitch: experimental measurements on slowly rotating baseballs *Am. J. Phys.* **82** 921–7
[4] Cobb T, Cobb W R and Dickson P 2009 *My Twenty Years in Baseball* (Mineola, NY: Dover)
[5] Nathan A M 2012 Analysis of knuckleball trajectories *Procedia Engineering* **34** 116–21
[6] Asai T, Ito S, Seo K and Hitotsubashi A 2010 Aerodynamics of a new volleyball *Procedia Engineering* **2** 2493–8
[7] Deprá P, Brenzikofer R, Goes M and Barros R 1998 Fluid mechanics analysis in volleyball services *16 International Symposium on Biomechanics in Sports* 85–8
[8] Barber S, Chin S B and Carré M J 2009 Sports ball aerodynamics: a numerical study of the erratic motion of soccer balls *Comput. Fluids* **38** 1091–100
[9] Hong S and Asai T 2014 Effect of panel shape of soccer ball on its flight characteristics *Sci. Rep.* **4** 5068
[10] Mehta R D 2014 Fluid mechanics of cricket ball swing *19th Australasian Fluid Mechanics Conference*
[11] Texier B D, Cohen C, Dupeux G, Quéré D and Clanet C 2014 On the size of sports fields *New J. Phys.* **16** 033039
[12] Watts R G and Sawyer E 1975 Aerodynamics of a knuckleball *Am. J. Phys.* **43** 960–3
[13] Morrissey M P 2009 The aerodynamics of the knuckleball pitch: an experimental investigation into the effects that the seam and slow rotation have on a baseball *Master's Thesis* Marquette University, paper 8 (http://epublications.marquette.edu/theses_open/8)
[14] Achenbach E 1974 Vortex shedding from spheres *J. Fluid Mech.* **62** 209–21
[15] Briggs L J 1959 Effect of spin and speed on the lateral deflection (curve) of a baseball; and the magnus effect for smooth spheres *Am. J. Phys.* **27** 589–96
[16] Mehta R D 1985 Aerodynamics of sports balls *Ann. Rev. Fluid Mechanics* **17** 151–89
[17] Achenbach E 1972 Experiments on the flow past spheres at very high reynolds numbers *J. Fluid Mech.* **54** 565–75
[18] Cohen C, Texier B D, Dupeux G, Brunel E, Quéré D and Clanet C 2014 The aerodynamic wall *Proc. R. Soc.* A **470** 20130497
[19] Norman A K and McKeon B J 2011 Unsteady force measurements in sphere flow from subcritical to supercritical reynolds numbers *Exp. Fluids* **51** 1439–53
[20] Horowitz M and Williamson CH K 2010 The effect of reynolds number on the dynamics and wakes of freely rising and falling spheres *J. Fluid Mech.* **651** 251–94
[21] Ern P, Risso F, Fabre D and Magnaudet J 2012 Wake-induced oscillatory paths of bodies freely rising or falling in fluids *Ann. Rev. Fluid Mechanics* **44** 97–121
[22] Brody H 1981 Physics of a tennis racket: the sweet spot *Am. J. Phys.* **49** 816–9
[23] Brody H 1986 The sweet spot of a baseball bat *Am. J. Phys.* **54** 640–3
[24] Achenbach E 1974 The effects of surface roughness and tunnel blockage on the flow past spheres *J. Fluid Mech.* **65** 113–25
[25] Mizota T, Kurogi K, Ohya Y, Okajima A, Naruo T and Kawamura Y 2013 The strange flight behaviour of slowly spinning soccer balls *Sci. Rep.* **3** 1871